



Using Full and Partial Unmixing Algorithms to Estimate the Inundation Extent of Small, Isolated Stock Ponds in an Arid Landscape

Christopher J. Jarchow¹  · Brent H. Sigafus² · Erin Muths³ · Blake R. Hossack⁴

Received: 4 October 2018 / Accepted: 4 July 2019

© This is a U.S. government work and not under copyright protection in the U.S.; foreign copyright protection may apply [YEAR] 2019

Abstract

Many natural wetlands around the world have disappeared or been replaced, resulting in the dependence of many wildlife species on small, artificial earthen stock ponds. These ponds provide critical wildlife habitat, such that the accurate detection of water and assessment of inundation extent is required. We applied a full (linear spectral mixture analysis; LSMA) and partial (matched filtering; MF) spectral unmixing algorithm to a 2007 Landsat 5 and a 2014 Landsat 8 satellite image to determine the ability of a time-intensive (i.e., more spectral input; LSMA) vs. a more efficient (less spectral input; MF) spectral unmixing approach to detect and estimate surface water area of stock ponds in southern Arizona, USA and northern Sonora, Mexico. Spearman rank correlations (r_s) between modeled and actual inundation areas less than a single Landsat pixel ($< 900 \text{ m}^2$) were low for both techniques (r_s range = 0.22 to 0.62), but improved for inundation areas $> 900 \text{ m}^2$ (r_s range = 0.34 to 0.70). Our results demonstrate that the MF approach can model ranked inundation extent of known pond locations with results comparable to or better than LSMA, but further refinement is required for estimating absolute inundation areas and mapping wetlands < 1 Landsat pixel.

Keywords Remote sensing · Spectral mixture analysis · Matched filtering · Stock ponds · Wetlands

Introduction

Accurately mapping and tracking variation in water is critical for resource management, including planning water use, identifying areas of concern for aquatic-borne diseases or vectors, and predicting risks for aquatic and semi-aquatic species (MEA 2005; Kalluri et al. 2007; Chandler et al.

2015). However, hydrologic monitoring data of small lentic waterbodies, including wetlands, is rare (*in situ* and *in silico*). Further, many wetlands are small and difficult to map with publicly available remote sensing data and technology because of limitations in temporal and spatial resolution. Although small wetlands of all sizes perform crucial ecosystem services and can increase local and regional biodiversity (Williams et al. 2003; Scheffer et al. 2006), our limited ability to characterize their hydrologic dynamics with remotely sensed data restricts management advances and efficiency (MEA 2005; Mitsch and Gosselink 2007; Halabisky et al. 2016).

In many arid areas, artificial impoundments (earthen stock ponds) support free-ranging livestock and have replaced natural wetlands (González-Bernal et al. 2012; Davies et al. 2013). These stock ponds now provide habitat to numerous species that might otherwise have disappeared from the landscape. For example, in the southwest USA, federally-threatened or -endangered species such as the Sonoran tiger salamander (*Ambystoma mavortium stebbinsi*) and Chiricahua leopard frog (*Rana chiricahuensis*) now depend almost

✉ Christopher J. Jarchow
christoj@email.arizona.edu

¹ Biosystems Engineering, University of Arizona, 1177 E. 4th St., Tucson, AZ 85719, USA

² U.S. Geological Survey, Southwest Biological Science Center, University of Arizona, 520 N. Park Avenue, Tucson, AZ 85719, USA

³ U.S. Geological Survey, Fort Collins Science Center, 2150 Center Ave. Bldg. C, Fort Collins, CO 80526, USA

⁴ U.S. Geological Survey, Northern Rocky Mountain Science Center, 800 E. Beckwith Ave., Missoula, MT 59801, USA

exclusively on earthen stock ponds for their persistence (Jarchow et al. 2016; Hossack et al. 2017). Many common game birds and large mammals also depend on these artificial wetlands (Krausman et al. 2006). Although stock ponds and other small wetlands are vital sources of water and provide critical wildlife habitat, their prevalence over vast expanses of land often makes ground-based monitoring of water presence or inundation extent infeasible. Also, the unpredictable and localized nature of storms in arid regions makes it especially difficult to predict which sites may contain water.

Remote sensing to monitor or detect water at the landscape-scale is a promising alternative to ground-based monitoring, with the added ability to track historic fill-and-dry cycles using archived satellite imagery; however, stock ponds tend to be small and isolated, limiting analyses of these sites to imagery with high spatial resolution (usually ≤ 1 m). Unfortunately, high spatial resolution imagery tends to be costly and limited in geographic and temporal coverage, precluding the ability to monitor sites consistently through time (Tiner 1990; Gallant 2015). As a result, such studies have been limited to a small number of dates and geographic areas (Van Dyke and Wasson 2005). The Landsat suite of satellites, on the other hand, provides a robust, moderate spatial (30 m) and temporal (16-d repeat) resolution archive of publicly-available imagery dating back over 30 years. This archive of historic imagery provides the ability to track long-term wetland fill-and-dry cycles in 8- to 16-d increments on a global scale (e.g., Pekel et al. 2016), but at the cost of a moderate resolution sensor.

Common remote sensing techniques for classifying land cover of Landsat or other imagery can be categorized as ‘soft’ or ‘hard’. Soft classification techniques include indices that leverage differences in reflectance properties of different bands (e.g., the Normalized Difference Water Index; McFeeters 1996), while hard classification techniques (e.g., Maximum Likelihood Classification) assign pixels to a particular class as defined during a training stage of the classification process (Foody 2000). Because hard classification techniques typically assume full membership of a given land cover type to an individual pixel, they tend to misrepresent true land cover in mixed-pixel situations (i.e., where land cover is not homogenous; Campbell 1996; Foody 2000). Coarser resolution sensors such as Landsat (pixel size = 900 m²) include a larger per-pixel footprint and are more likely to contain more than one land cover type in a given pixel. For mapping wetlands, this can be particularly problematic, as many isolated wetlands are smaller than the area of a Landsat pixel (e.g., Halabiskiy et al. 2016; Hossack et al. 2017).

To accurately classify these sub-pixel sized wetlands, methods such as regression trees (Rover et al. 2010; Huang et al. 2014; Jin et al. 2017) and discrete particle swarm optimization (Li et al. 2015a) have been used. Another method that provides a potential solution to the mixed pixel problem

and mapping of sub-pixel wetlands is spectral unmixing. For example, linear spectral mixture analysis (LSMA) is a full unmixing method that estimates the relative abundance of individual components (spectral endmembers) in the landscape based on their unique spectral characteristics (Hu et al. 1999; Heinz and Chang 2001) and has been used to map a variety of features, including crop residues, land cover degradation, lava flows, forest cover, and impervious surfaces (Bannari et al. 2006; Lu and Weng 2006; Li et al. 2015b; Mayes et al. 2015; Sun and Liu 2015). In LSMA, the spectral signature of a given pixel is assumed to be the linear superposition of all significant endmembers within that pixel. As such, the fractional abundance of each endmember is estimated on a pixel-by-pixel basis, allowing for the conversion of fractional abundance to surface area based on the dimensions of the pixel (Halabiskiy et al. 2016).

Despite the potential of LSMA for estimating surface water area at sub-Landsat pixel scales (e.g., Rover et al. 2010; Halabiskiy et al. 2016), it has a few key limitations that can preclude its application in certain areas or under certain conditions. First, it requires *a priori* knowledge of pure spectra of each endmember either from the image itself, a spectral library, or from *in situ* measurements. Second, all scene-significant endmembers must be represented (Nielsen 2001). Finally, the number of endmembers used must be less than the number of spectral bands in the image(s), limiting applicability with multiband sensors like Landsat (as opposed to hyperspectral data; Nielsen 2001). Identification of all scene-significant endmembers, in particular, can be time consuming and based largely on trial-and-error (Van Der Meer 1999).

Matched filtering (MF; a partial unmixing approach; Boardman et al. 1995; Mundt et al. 2007) provides a potentially more efficient alternative to full spectral unmixing techniques when the user is only interested in a single endmember. Unlike full unmixing algorithms, partial unmixing only requires one target endmember (Frohn et al. 2012), eliminating the time required to identify all significant endmembers in a given scene. In this approach, the response by the target endmember is enhanced, while the unknown composite background (unknown endmembers) is ignored (Boardman et al. 1995; Mundt et al. 2007; Frohn et al. 2012). Matched filtering estimates approximate sub-pixel abundance, but only for the endmember of interest, allowing for the estimation of surface area covered by the target endmember (e.g., water) on a pixel-by-pixel basis.

Matched filtering has been used to detect wetlands ranging in size from $\sim 2,000$ m² to $>1,200,000$ m² (e.g., Roshier and Rumbachs 2004; Frohn et al. 2012). To our knowledge, the efficacy of this approach to explicitly estimate inundation extent (and hydroperiod by extension) of small (defined here as <900 m²), isolated wetlands has not been assessed. Our objective was to compare the ability of MF and LSMA to map such sites using Landsat 5 Thematic Mapper (TM) and

Landsat 8 Operational Land Imager (OLI) data. We analyzed 81 stock ponds corresponding to a 2007 Landsat 5 image and 73 sites corresponding to a 2014 Landsat 8 image in southern Arizona and northern Sonora, Mexico, with ponds ranging from completely dry to $\sim 17,000 \text{ m}^2$ surface water.

Methods

Study Area

We assessed the inundation extent of stock ponds in the San Rafael Valley and surrounding areas. The northern part of the valley is in Santa Cruz County, Arizona, and extends into the northern part of Sonora, Mexico. The area ranges from $\sim 1,400$ to 1,500 m in elevation, with surrounding mountains $>1,800$ m. Annual precipitation averages ~ 438 mm in the valley, with the majority (~ 270 mm) of rainfall occurring during the summer monsoon season (ADWR 2014). The San Rafael Valley is predominately flat grassland, transitioning into riparian deciduous and Madrean evergreen woodland near the surrounding mountains (Arizona State Parks n.d.). Human activities such as groundwater pumping have severely reduced surface water in this area. As with many arid and semi-arid rangelands in western North America, earthen stock ponds are common in the San Rafael Valley. These ponds were designed to catch and retain upstream runoff during rain events and are typically isolated from one another; however, their ability to retain water varies considerably, with some holding water year-round (perennially) and others only intermittently.

Stock Pond Selection

We developed a database of stock ponds in the project area using a combination of ground data, high resolution imagery, and a 1:24,000 scale topographic map (used to locate ponds) via the Basemap function in ArcGIS v10.3 (Fig. 1). Using the high resolution basemap imagery (< 1 m) and ground-based GPS data, we digitized the high-water line (max. inundation extent) of every stock pond identified in our project area. The high water line was visible as a line of woody trees or a distinct change in soil coloration along the perimeter of the pond, which was also supported by ground observations. We digitized 154 ponds ranging from 680 m^2 to $17,442 \text{ m}^2$. We located additional sites, but removed ponds lacking a distinct high water line, inundated ponds with water visually indistinguishable from soil, and ponds $< 600 \text{ m}^2$ (area within high water line, not inundation extent) to reduce misclassification errors (Halabisky et al. 2016).

Validation Imagery

Since our objective was to validate a technique for estimating the surface water area of small, isolated wetlands from the long-term Landsat record, we used high resolution images to validate the Landsat images. The image we chose for Landsat 5 validation was a 1 m resolution National Agriculture Imagery Program (NAIP) scene captured 25 June 2007, which corresponded to a Landsat 5 image captured 27 June 2007 (see Table 1 for image details). This was the closest acquisition period we could locate for our study area. The NAIP image was mostly restricted to the US portion of the study area (Fig. 1). For Landsat 8, we used a DigitalGlobe WorldView-2 (WV-2) 0.5 m resolution image captured 21 May 2014 and a Landsat image from 22 May 2014. This validation image extended farther south and east than NAIP (Fig. 1). Despite differences between the Landsat and validation scene capture dates (2-d for Landsat 5 and 1-d for Landsat 8), no precipitation was recorded at nearby weather stations during these periods; therefore, it is unlikely inundation areas increased during this time, but we could not account for water lost through evaporation or infiltration into the ground.

Both Landsat images we used were Tier 1 Level-1 terrain-corrected scenes acquired from EarthExplorer (<https://earthexplorer.usgs.gov>), which were provided as individual bands represented by digital numbers (DNs). Atmospheric correction was not used because it is not needed if the geographic extent is limited and endmembers are selected directly from the scenes themselves (Aspinall et al. 2002). Atmospheric effects are assumed to be uniform across small areas, thereby allowing features to appear similar across the entire study area (Aspinall et al. 2002). Despite this, we initially used atmospherically corrected (surface reflectance) Landsat scenes (not shown), but results were poorer than with the uncorrected imagery (Fig. 2). To maintain consistent spatial and spectral resolution between platforms, we excluded Band 6 (Thermal) from Landsat 5 and Bands 1 (Ultra-Blue), 8 (Panchromatic), 9 (Cirrus), 10 (Thermal Infrared 1), and 11 (Thermal Infrared 2) from Landsat 8 (Halabisky et al. 2016). We subsequently composited the bands and clipped the scenes to the study boundary. See Table 1 for additional scene details.

Validation Stock Ponds

Using each high resolution validation image described in Section 2.3 and the identified stock ponds (Section 2.2), we visually surveyed each digitized stock pond. If water was present, we digitized the perimeter of the inundation area. Because the WorldView-2 validation image contained clouds that covered some sampling sites, we extended the sampling extent south into Mexico and farther east compared to the NAIP sampling area (Fig. 1), resulting in a different number of sampling sites between periods

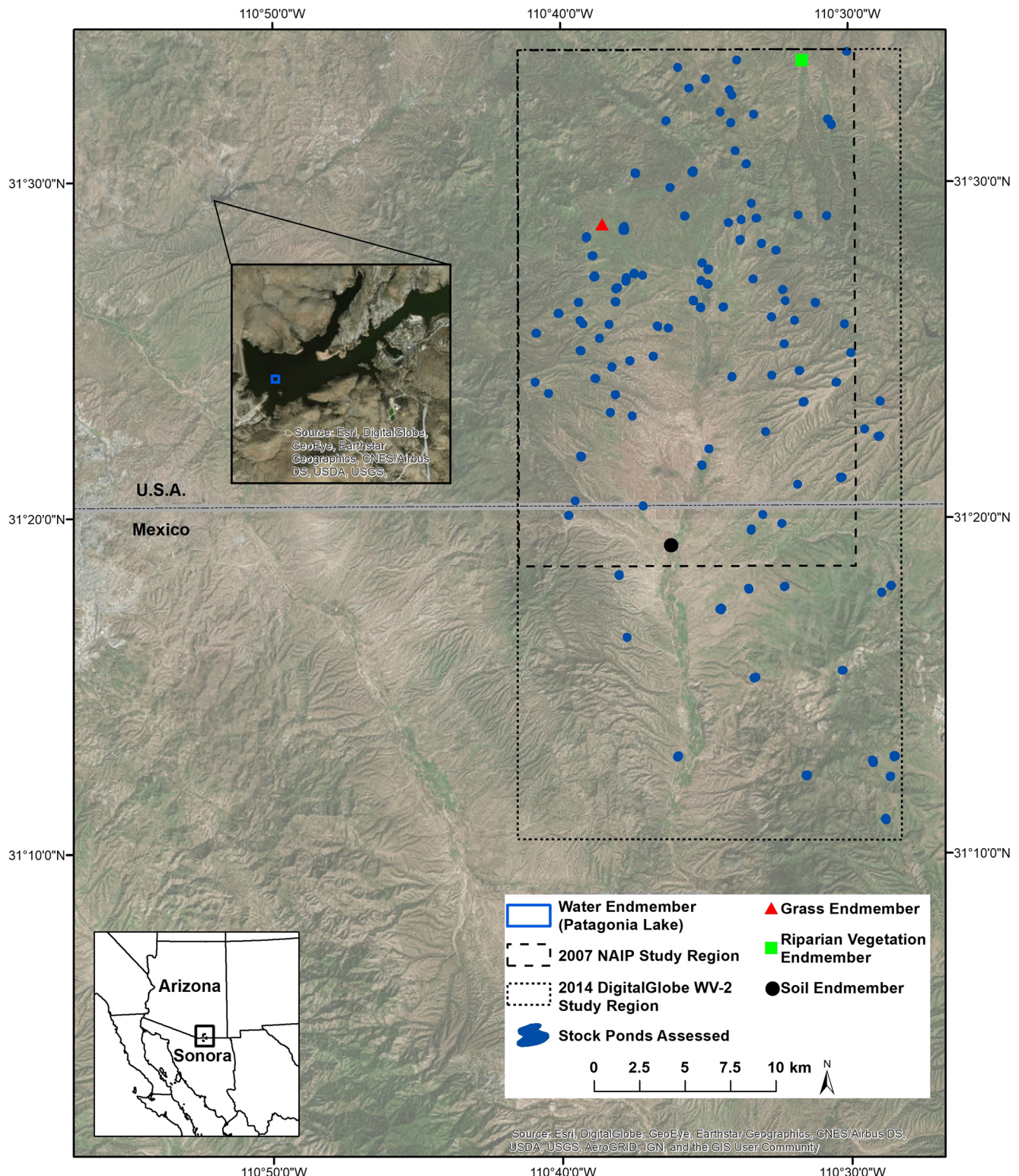


Fig. 1 Study regions, endmember sampling locations, and stock ponds sampled for the 2007 validation period (corresponding to Landsat 5 Thematic Mapper; TM) and 2014 validation period (Landsat 8 Operational Land Imager; OLI)

(sensors; Table 1). For the 2007 validation period, 41 of the 56 inundated ponds had inundation extents $<900 \text{ m}^2$, while 25 of 40 inundated ponds for the 2014 period had

inundation extents $<900 \text{ m}^2$. We buffered the outer boundary of all stock ponds by 30 m to account for small pixel shifts between images and then converted these buffered

Table 1 Dry and inundated sites sampled for each validation image (period)

Landsat sensor	Validation image	Landsat acquisition date	Validation acquisition date	Dry ponds (n)	Inundated ponds (n)	Inundation extent (m^2)	Mean inundation extent (m^2)	PDSI
Landsat 5 TM	NAIP	27 Jun. 2007	25 Jun. 2007	25	56	113–17,442	1,110	≤ -4.0
Landsat 8 OLI	DigitalGlobe WV-2	22 May 2014	21 May 2014	33	40	249–6,194	1,216	-3.0 to -3.9

The Palmer Drought Severity Index (PDSI) for the corresponding week is also given (<http://www.cpc.ncep.noaa.gov>)

perimeters to 30 m rasters for subsequent analysis (Halabiskiy et al. 2016).

Matched Filtering and Linear Spectral Mixture Analysis

All spectral analyses and data extraction were performed in ENVI v5.0. For MF and LSMA, we extracted our water endmember from Patagonia Lake, the largest water source in our area (Figs. 1 and 2). We chose Patagonia Lake because the inundation extents of stock ponds in our study area were too small to contain pixels of pure water, a requirement of spectral unmixing. Furthermore, we were unable to select water endmembers that may have better represented some of the conditions associated with stock ponds (e.g., muddy or algal

water) because we were limited to a large body of water in the area, which did not exhibit such spectral characteristics. Following Halabiskiy et al. (2016), we used three additional endmembers that represented dominant (scene-significant) land cover types in our area: riparian vegetation (verdant trees, in this case), bare soil, and grass. Spectrally pure pixels of all endmembers were identified in or near the study region using the high resolution validation imagery corresponding to the Landsat 8 OLI and Landsat 5 TM time periods.

To extract spectra for the endmembers described above, we first digitized a vector polygon corresponding to the spectrally pure Landsat pixel, then created a Region of Interest (ROI) for each scene (Landsat 5 TM and Landsat 8 OLI). We then viewed and saved the ROI Stats for each endmember. We applied these spectral stats files to each Landsat scene using

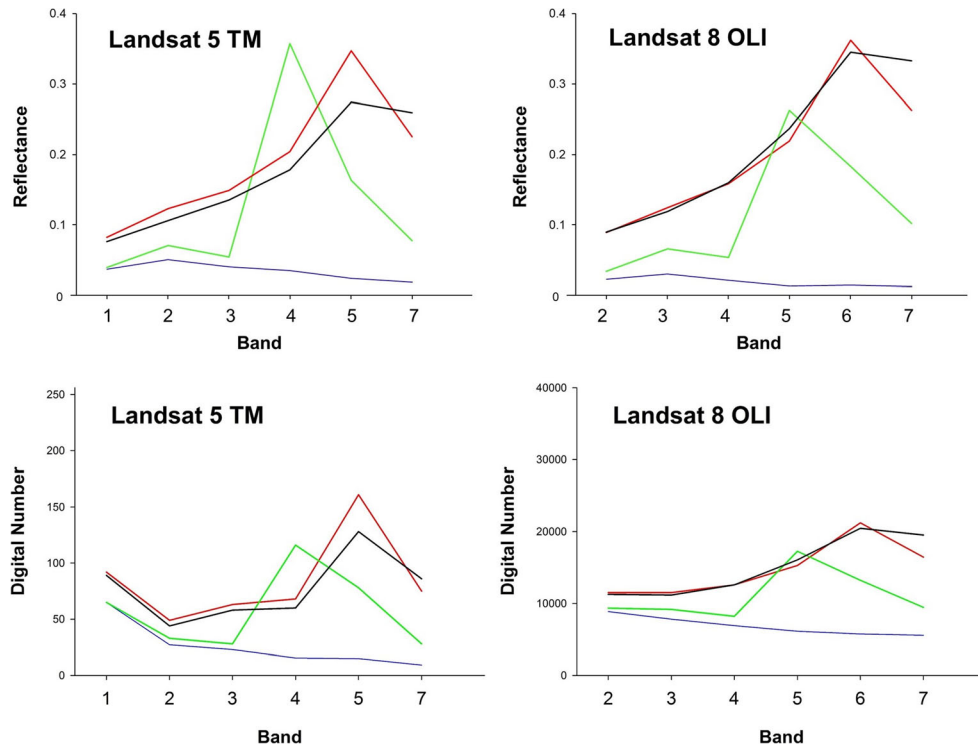


Fig. 2 Spectral curves of the water (blue), riparian vegetation (green), grass (red), and soil (black) endmembers chosen for modeling of Landsat 5 Thematic Mapper (TM) and Landsat 8 Operational Land Imager (OLI) imagery. (Top) Endmembers extracted from atmospherically corrected (surface reflectance) images (not used in our analysis). Surface reflectance was based on the Landsat Ecosystem

Disturbance Adaptive Processing System (LEDAPS) for Landsat 5 and Landsat 8 Surface Reflectance Code (LaSRC) provided by the U.S. Geological Survey. (Bottom) Endmembers extracted from uncorrected imagery used in the current study. Digital number values and ranges differ between sensors due to differences in dynamic ranges (8-bit for Landsat 5 TM and 16-bit for Landsat 8 OLI)

Matched Filtering and Linear Spectral Unmixing. For Linear Spectral Unmixing, we used a sum constraint of 10,000 (Halabisky et al. 2016), producing rasters that represented the fractional abundance of each endmember on a per-pixel basis. Unlike LSMA, the MF technique does not employ a sum-to-one constraint (Mundt et al. 2007). Values ranged from <0.0 to ~1.0, where values ≤0.0 theoretically represented cells lacking the target endmember and values >0.0 represented the fractional amount of the cell covered by that endmember, with ~1.0 representing a perfect match to the target material (e.g., 100% water). The output of the MF process was a single raster representing the target endmember (water), while LSMA produced five rasters (four abundance images of each endmember and a root mean square [RMS] error surface). Because we were interested in water, we only exported the water and RMS raster from the LSMA output. To estimate the surface area of water on a pixel-by-pixel basis, we converted cell values <0.0 to 0.0 (resulting in a range of 0.0 to ~1.0) and multiplied each cell by 900 m² (the area of a single Landsat pixel), resulting in the area of each Landsat pixel covered by water.

Surface Water Area Validation

We used the MF and LSMA surface water area rasters and the buffered stock ponds for each Landsat 5 and Landsat 8 image to determine the accuracy of these techniques for estimating the area of surface water (inundation extent) at each site. Since

we previously converted the output into area of water per cell, we summed the area of water for all cells falling within the buffered boundary of each selected stock pond. This can be described as:

$$\sum_{i=1}^n F_i * a \quad (1)$$

where F is the fractional abundance of water for pixel i , a is the area of a single Landsat pixel, and n is the number of pixels for each stock pond (Halabisky et al. 2016). Limiting our analysis to the buffered region of each stock pond also reduced the likelihood of including false positives (commission errors). We then compared the modeled output to the actual inundation area digitized for each stock pond (from the layer described in Section 2.4). In this manner, stock ponds could range from completely dry to completely inundated.

Statistical Procedures

Due to large outliers, large number of zero values, and non-constant variance in the data set (see Figs. 3 and 4), we used Spearman's rank correlation coefficient (r_s) to assess the strength of association between actual inundation extent and modeled extents. Since we suspected pixel size would be a limiting factor in modelling inundation extent, we further divided the analysis by inundation extents above and below 900 m². To assess the ability of MF and LSMA to accurately model inundation extent and determine if these techniques

Fig. 3 Comparison of modeled surface water area as derived from the MF (matched filtering) and LSMA (linear spectral mixture analysis) method against actual surface area for the 2007 and 2014 Landsat validation periods. Spearman rank correlations (r_s) were used to assess associations between actual and modeled surface water area. Insets and 1:1 lines are shown here for ease of interpretation

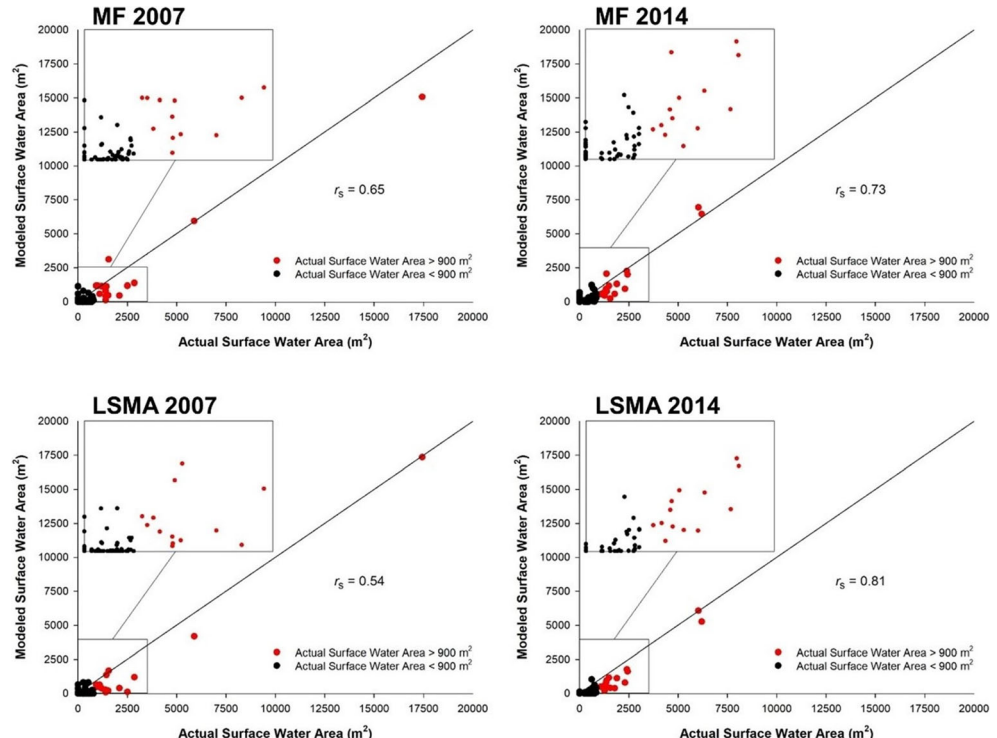
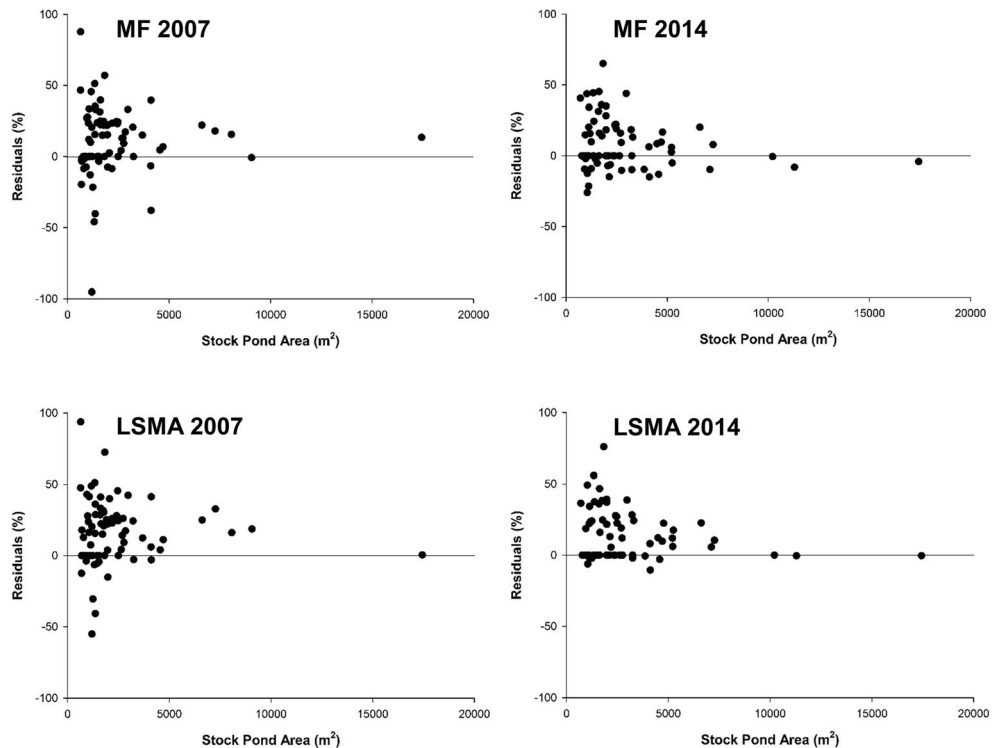


Fig. 4 Residuals of relationship between percent modeled (predicted by matched filtering (MF) and linear spectral mixture analysis (LSMA)) inundation extent and percent actual inundation extent for the 2007 and 2014 Landsat validation images. The stock pond area, as determined by the high water line, is plotted on the x-axes



over or underestimated this parameter, we calculated bias (mean error) as:

$$\text{Bias} = \frac{1}{n} \sum_{i=1}^n (m_i - a_i) \quad (2)$$

where m is the modeled surface water area and a is the actual surface water area of each stock pond as estimated using the high resolution validation images. We calculated the actual and modeled percent inundation of each stock pond and plotted the residuals against stock pond size to determine if error changed with the maximum area of each site. We used the RMS error rasters from the 2007 and 2014 Landsat LSMA ENVI outputs to assess noise within the stock ponds (mean pixel RMS error).

Results

Matched Filtering

Overall, the association between modeled and actual surface water area was moderately strong for the 2007 validation

period ($r_s = 0.65$; $P < 0.001$; bias = -254.85 m^2 ; $n = 81$; Fig. 3; Table 2); however, the relationship was weaker for inundation extents $<900 \text{ m}^2$ ($r_s = 0.39$; bias = -169.81 m^2) or $>900 \text{ m}^2$ ($r_s = 0.46$; bias = -629.03 m^2 ; Fig. 3; Table 2). Of the 25 dry sites, 10 (40%) were misclassified as having water present, while 14 of the 41 (34.15%) inundated sites with $<900 \text{ m}^2$ actual surface water were misclassified as dry. All sites $>900 \text{ m}^2$ were correctly predicted to have water. Prediction error was inversely related to pond size, as indicated by larger residuals for ponds $<900 \text{ m}^2$ (Fig. 4).

The association between modeled and actual surface water area for Landsat 8 (2014) was stronger than that for Landsat 5 ($r_s = 0.73$; $P < 0.001$; bias = -141.51 m^2 ; $n = 73$; Fig. 3; Table 2). Modeled data from Landsat 8 were more highly correlated with actual surface water areas $>900 \text{ m}^2$ ($r_s = 0.70$; bias = -416.91 ; Fig. 3; Table 2) compared to sites with actual inundation areas $<900 \text{ m}^2$ ($r_s = 0.51$; bias = -70.29 m^2), with greater error for small ponds (Fig. 4). Of the 33 dry sites, 17 (51.52%) were misclassified as having water present, while 2 of the 25 (8.00%) inundated sites with $<900 \text{ m}^2$ actual surface water were misclassified as dry. All sites $>900 \text{ m}^2$ were correctly predicted to have water.

Table 2 Spearman rank correlations (r_s) between modeled and actual stock pond inundation extents for matched filtering (MF) and linear spectral mixture analysis (LSMA)

Method	Year	Landsat Sensor	r_s (All Ponds)	r_s (Inundation $<900 \text{ m}^2$)	r_s (Inundation $>900 \text{ m}^2$)
MF	2007	Landsat 5 TM	0.65	0.39	0.46
LSMA	2007	Landsat 5 TM	0.54	0.22	0.34
MF	2014	Landsat 8 OLI	0.73	0.51	0.70
LSMA	2014	Landsat 8 OLI	0.81	0.62	0.70

Linear Spectral Mixture Analysis

Our LSMA results for the 2007 validation period were similar to our MF results for all sites ($r_s = 0.54$; $P < 0.001$; bias = -345.02 m^2 ; Fig. 3; Table 2), with a low correlation between modeled and actual surface water areas $<900 \text{ m}^2$ ($r_s = 0.22$; bias = -203.85 m^2 ; Fig. 3; Table 2) and for actual surface water areas $>900 \text{ m}^2$ ($r_s = 0.34$; bias = -966.20 m^2 ; Fig. 3; Table 2). Error was greater for small ponds (Fig. 4). Of the 25 dry sites, 7 (28.00%) were misclassified as having water present, while 20 of the 41(48.78%) inundated sites with $<900 \text{ m}^2$ actual surface water were misclassified as dry. All sites $>900 \text{ m}^2$ were correctly predicted to have water. Average RMS error of stock ponds for the 2007 LSMA model ranged from 1.42 to 9.09 DNs, with a mean of 4.23 DNs.

Performance increased from 2007 (Landsat 5 TM) to 2014 (Landsat 8 OLI) during the LSMA, with an r_s of 0.81 for all sites ($P < 0.001$; bias = -294.18 m^2 ; Fig. 3; Table 2). The correlation between modeled and actual surface water areas $<900 \text{ m}^2$ was strongest for this subset of sites and method ($r_s = 0.62$; bias = -170.50 m^2 ; Fig. 3; Table 2) and increased for inundation extents $>900 \text{ m}^2$ ($r_s = 0.70$; bias = -772.44 m^2 ; Fig. 3; Table 2). Of the 33 dry sites, 8 (24.24%) were misclassified as having water present, while 7 of the 25 (28.00%) inundated sites with $<900 \text{ m}^2$ actual surface water were misclassified as dry. All sites $>900 \text{ m}^2$ were correctly predicted to have water. RMS error of stock ponds ranged from 173.20 to 1,088.67 DNs, with a mean of 502.87 DNs.

Discussion

Significance

Our study compared and evaluated a full (LSMA; less efficient) and partial (MF; more efficient) unmixing technique for assessing the inundation extent of small waterbodies; however, it is important to note that efficient refers to time spent obtaining the input information required of the two unmixing techniques. We generally assume less time would be required to gather spectral information of a single endmember of interest (MF), compared to multiple, scene-significant endmembers (LSMA). Neither method reliably mapped sub-pixel sized wetlands, but our results demonstrate that MF can be used to model ranked size of inundation extent, with results comparable to, and in some cases better than LSMA. We build upon prior attempts to map wetlands using spectral unmixing techniques, demonstrating that MF-based inundation extents can be correlated with actual surface water area.

We found no clear benefit to using the less efficient full unmixing algorithm (LSMA) over the more efficient partial approach (MF). In contrast to our findings, Halabisky et al. 2016 found that a four-endmember LSMA yielded a 99%

correlation between modeled and actual surface water areas, with inundation extents ranging from completely dry to $>220,000 \text{ m}^2$. The difference in outcomes between the current study and Halabisky et al. (2016) likely highlights the importance of extracting the correct endmember spectra for LSMA analysis (described in Section 4.2) and the potential of this technique to be highly accurate when scene-significant endmembers are correctly identified. The tradeoff to this, however, is that high accuracy can be time-intensive, as it can require significant time to correctly identify all scene-significant input spectra. As such, LSMA may not be a practical method for resource managers when time, remote sensing expertise, or funding is limited.

More recently, cloud-hosting services have enabled researchers to successfully map surface water on a global scale using the full Landsat archive (e.g., Donchyts et al. 2016; Pekel et al. 2016). While these mapping efforts provide valuable information regarding long-term, global-scale changes in surface water dynamics, they were not reliable for many of the small, spectrally altered waterbodies observed in our study area. This illustrates the need for regionally targeted mapping efforts, especially for very small (sub-pixel), spectrally diverse waterbodies. While the techniques in our study are not novel, we demonstrate that mapping these small, isolated water sources presents a unique challenge that requires further investigation. Such efforts will be crucial to managing sensitive wildlife species in arid and semi-arid regions of the world.

Error, Limitations, and Requirements

One major limitation in our study was the use of digital numbers (DNs) instead of surface reflectance data. As mentioned previously, surface reflectance imagery did not provide an advantage over uncorrected imagery. While this may seem counterintuitive, it is not unusual in the mapping of inland, spectrally complex waterbodies. Atmospheric correction of these aquatic environments is particularly challenging because of terrestrial sources of atmospheric pollution that can cause optical heterogeneity; land-adjacency effects that can contaminate the signal received by the sensor; and high sediment concentrations that can cause increased reflectance in the near-infrared, making it difficult to remove the effect of atmospheric aerosol scattering (Moses et al. 2017). The latter can lead to overcorrection in shorter wavelengths, resulting in erroneously low values.

Additionally, because Landsat 8 Surface Reflectance Code (LaSRC) uses the blue band for aerosol inversion tests, this band should not be used for analysis (USGS 2018), potentially explaining poorer performance in our study. The pattern we observed for our water endmember (Fig. 2) was similar to that reported by Ilori et al. (2019), who found that Landsat 8 surface reflectance performed unreliably in the blue wavelengths over coastal waters. The terrestrial Landsat 8 LaSRC has also

demonstrated poor performance in turbid conditions (conditions common to the sites we studied; Ilori et al. 2019), where water atmospheric correction routines might be more suitable (Wang et al. 2019). Regarding Landsat 5, Torbick et al. (2013) found that DN models generally outranked those based on Landsat Ecosystem Disturbance Adaptive Processing System (LEDAPS) atmospheric correction when used to model water quality of inland lakes. Therefore, the terrestrial LEDAPS and LaSRC Landsat products we initially used (Fig. 2) might not be suitable for the waterbodies or environmental conditions we studied.

The use of DNs, however, restricts analyses over time and space and requires spectral endmembers to be extracted from each individual scene or region(s) analyzed. Atmospheric correction can potentially remove these temporal and geographic limitations, but accurate surface reflectance over spectrally complex inland waters is characteristically difficult to achieve, and further development of land and water atmospheric correction routines are needed to improve performance in these areas (Wang et al. 2019). Based on the conditions characterizing the sites we studied, several land and water atmospheric correction techniques should be tested to determine the best performing routine for resolving complex atmospheric and aquatic conditions.

Several potential sources of error or limitations in our approach reduced the accuracy of our estimation of inundation extent in our study area. One major challenge was the difference in spectra between Patagonia Lake and some of the stock ponds. While the water spectra we chose followed a typical reflectance curve for clear water (Fig. 2), the color of the water in stock ponds as viewed in the validation images varied from a typical dark color to turbid (muddy) or algal (green; Fig. 5). At the wavelengths measured by Landsat 5 TM and 8 OLI, the spectral properties of water can vary with suspended solids, chlorophyll concentration, water depth, and the substrate of shallow waterbodies (factors commonly encountered in stock ponds; Arst 2003). Higher error rates have been found in wetlands with emergent vegetation (DeVries et al. 2017), which could be spectrally analogous to ponds with high algal loads or floating vegetation (also common in stock ponds). We suspect the water endmember from Patagonia Lake did not adequately match the spectral nature of many of the stock ponds we sampled.

A challenge with the LSMA technique is that failing to select all significant endmembers for the area(s) of interest can produce increased noise in the resulting RMS error images (Van Der Meer 1999). Nichol and Vohora (2004) suggested that an acceptable level of noise for Landsat 5 data was <2 DNs, indicating that our Landsat 5 TM modeling results may have misrepresented the spectral dimensionality and spectral variability of the image (Van Der Meer 1999). Because Landsat 5 TM and Landsat 8 OLI have different dynamic ranges, this rule cannot be directly applied to our Landsat 8

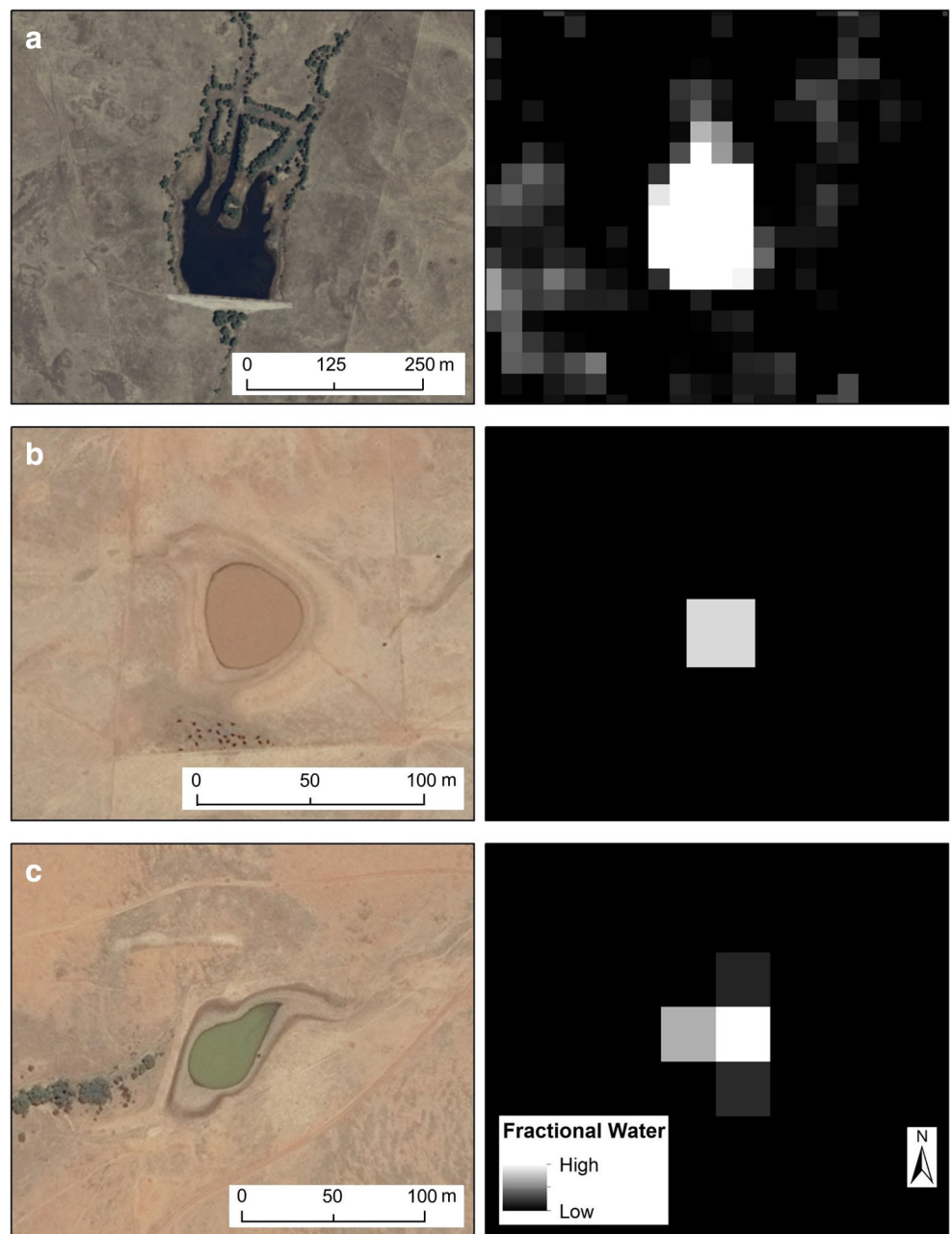
LSMA results; however, on a proportional basis, our mean RMS error for OLI was below this threshold. Using different sets of endmembers (locations and materials in the landscape; not shown) to select scene-significant endmembers resulted in poorer estimates of fractional water. Factoring in the time to search for these endmembers, we estimate LSMA was at least twice as time-intensive as MF.

The differences in spatial resolution between validation images (1 m in 2007 and 0.5 m in 2014) and Landsat scene capture dates (2-d in 2007 and 1-d in 2014) could have also contributed to weaker correlations in 2007 compared to 2014 for both MF and LSMA. While evaporation rates were expected to be relatively constant across the study area, infiltration rates are less predictable and likely differed between sites, possibly leading to the variability observed in 2007. Therefore, we suspect the 2014 results likely more accurately reflect the ability of MF and LSMA to accurately model inundation extent. Additionally, based on mean inundation extent and the Palmer Drought Severity Index (Table 1), slightly wetter conditions in 2014 could have contributed to a stronger correlation. Landsat 8's higher bit-depth and improved signal-to-noise ratio also likely contributed to this difference in performance.

For both MF and LSMA, the magnitude of error was greater for small vs. large ponds, but error was slightly lower for Landsat 8 in 2014 compared to Landsat 5 in 2007. Because the scenes from these two platforms represented different time periods, the differences in accuracy might not be sensor-related. Likewise, because we focused on modeling surface water area within delineated stock ponds, we did not assess error outside these regions. Our observed error is consistent with Halabisky et al. (2016), who found that accuracy decreased for smaller wetlands; however, the magnitude of the residuals in our study ranged from -95.29% to $+93.77\%$, whereas their highest residual was 28%. False positive rates were high for MF and LSMA (mean pixel inundation = 14.74 m^2 , standard deviation = 31.11 m^2), making it difficult to accurately track water presence/absence for wetlands $<900 \text{ m}^2$.

Sub-pixel modeling methods may be most suitable in situations with low contrast between wetlands and surrounding areas, while a segmentation object-oriented approach is more appropriate for areas with high contrast (e.g., Frohn et al. 2012). As evident in Fig. 6b, we found high error rates in areas with low contrast. Halabisky et al. (2016) conducted their analysis in a high contrast landscape with little topographic relief and suggested non-spectrally pure water (e.g., water containing algae) could have affected their sub-pixel analysis. Some of our sites were obscured by shadows from trees and steep topography, which tend to be spectrally similar to water. Fractional estimates of water surface area for these sites were erroneously high (Fig. 6a-b). This was particularly pervasive in heavily vegetated areas, highlighting the importance of restricting analysis to the individual stock ponds. On the other

Fig. 5 Examples of water contained by different stock ponds in our study area as viewed in the validation image (left) and corresponding modeled (matched filtering) image (right). Water ranged from a typical dark signature (a) to turbid (b) or algal (c). Despite the fractional water visible in the corresponding modeled images, these fractions were not necessarily accurate

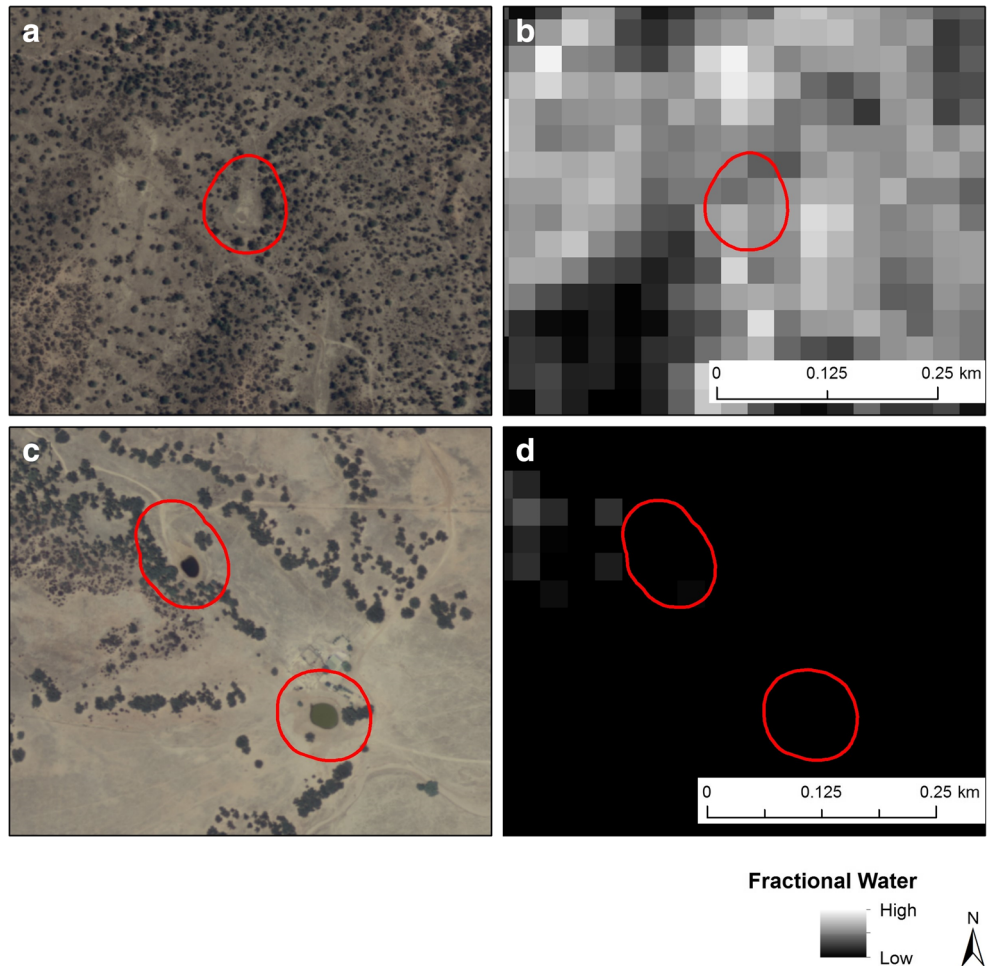


hand, in areas of the San Rafael Valley with subtle topography and minimal tree cover, some sites were falsely modeled as dry (Fig. 6c-d). Based on these misclassifications, the background spectra (e.g., of soil, shadows, or vegetation) might not provide adequate contrast to differentiate water from other features. Scenes acquired during the summer rainy season (monsoon season) could provide better unmixing results, as increased greening of vegetation could improve background contrast. Unfortunately, only pre-monsoonal validation images were available during the present study.

There are a few key limitations in the MF and LSMA approaches. First, our technique relies on the accurate delineation of stock pond boundaries (defined as the high

water line in this study), which can be affected by the quality and resolution of the imagery used in the classification or digitization process; however, because we eliminated sites that did not have well-defined boundaries, we do not suspect this had a significant effect on the outcome. Additionally, both partial and full unmixing algorithms require a pure water endmember, preferably near the project area. This can be difficult to obtain where surface water is scarce or where large water impoundments (e.g., man-made lakes) are uncommon. Since the only validation images we could locate for our area were acquired in early summer prior to the rainy season, it is unknown how seasonality may affect these results.

Fig. 6 Examples of misclassified pixels resulting from the matched filtering process. Image **a** shows a dry stock pond that was classified as having water (**b**). Image **c** shows two ponds containing water that were classified as dry (0% surface water; **d**)



Finally, and possibly the most challenging limitation in the current study, is having to exclude inundation areas $<900 \text{ m}^2$. Waterbodies $<900 \text{ m}^2$ are often abundant and ecologically significant (Gibbs 1993; Scheffer et al. 2006). For waterbodies that shrink below the 900 m^2 threshold seasonally, this limitation adds error to hydrologic modeling and adds to management uncertainty. For example, stock ponds in southern Arizona that are critical to the recovery of a reintroduced population of federally-threatened Chiricahua leopard frogs commonly fluctuate from $>4,000 \text{ m}^2$ to $<900 \text{ m}^2$ (Chandler et al. 2015; Jarchow et al. 2016). During some years, the ponds dry completely, but during other years they retain a small amount of water that would be undetectable using current remote sensing methods and commonly-available imagery such as Landsat. Dealing with this size limitation would require eliminating only the precise area of a site corresponding to the unique fill boundary less than this threshold value. Because the structure of the bottom (bathymetry) of such sites is usually unknown or impossible to map without expensive, high resolution data (e.g., LiDAR), it would be difficult to accurately remove areas with irregular boundaries or bathymetry. More recent satellite missions such as the European Space

Agency's Sentinel-2A and -2B satellites provide higher temporal (5-d combined) and spatial resolution (10 m) alternatives to Landsat and should improve our ability to map small waterbodies in the future, but without the historic depth of the Landsat record.

Applications

Our results suggest the MF approach can be a useful and efficient technique for modeling ranks of inundation extent for surface water areas $>900 \text{ m}^2$. With some spectral refinement, this method could be helpful for evaluating inter- and intra-annual changes in surface water over large areas, potentially spanning the entire Landsat 5 and Landsat 8 record (over 30 years of imagery); however, because stronger correlations were observed in 2014, it is possible this technique might be better suited to Landsat 8 data. Such data could be paired with precipitation data to understand the long-term effect of drought on surface water in relatively small, isolated water bodies, which would be particularly useful in regions where climate change is likely to exacerbate drought, such as in the Desert Southwest. Long-term fill-and-dry cycles could also be

used in conjunction with drought forecasting techniques to predict future surface water availability, which could inform planning of livestock operations as well as modeling of wildlife extinction risk and habitat connectivity (e.g., Chandler et al. 2015; Jarchow et al. 2016).

Because of Landsat's 16-d repeat cycle, our approach could also be used for monitoring surface water, allowing for adaptive management of water resources in near real-time (e.g., Jin et al. 2017). This would be particularly helpful for prioritizing management efforts of aquatic or semi-aquatic species, where animals may need to be translocated based on up-to-date water availability. For example, some species' recovery plans include strategies to identify and salvage populations from drying habitats or to deliver water to a site before it dries (USFWS 2007). With some refinement, current wetland extent could also be compared to historic extent to identify long-term trends important for maintaining wetland habitat and water quality, a common problem in anthropogenically altered landscapes (Papastergiadou et al. 2007).

Conclusion

We demonstrated that matched filtering (MF) can be used to estimate inundation extent of small ($\sim 900 \text{ m}^2$ to $>6,000 \text{ m}^2$) wetlands (stock ponds), with rank correlations comparable to or better than linear spectral mixture analysis (LSMA). Despite low correlations between modeled and actual inundation extents $<900 \text{ m}^2$ in this study (Spearman rank correlation (r_s) range = 0.22 to 0.62), estimates from both methods were moderately correlated for inundation areas greater than a single Landsat pixel in 2014 ($r_s = 0.70$). Because MF does not require knowledge of all significant endmembers of a given scene, it is an efficient alternative to LSMA; therefore, it can be a useful tool for resource managers interested in quickly mapping these features at a landscape level. But, we do not recommend this technique for estimating absolute (quantified) inundation areas nor for detecting water in small basins, as error rates were high. The spectral characteristics of the stock pond water and the surrounding landscape likely contributed to the inability to accurately estimate sub-pixel abundance of water in the area tested. To increase success of these spectral unmixing techniques, future efforts should include a comprehensive spectral characterization of the waterbodies being mapped, especially in optically complex waters. Accurate mapping of small wetlands is particularly important, as drought is expected to be exacerbated by climate change, increasing the importance of these resources to ecosystem services and wildlife.

Acknowledgements We thank Caren Goldberg for providing GPS locations of sampling sites and K. Stemp for acquiring satellite imagery. We also thank W. Lowe, T. Wilcox, B. Addis, R. Kovach, P. Garciasoto, M. Bayer, L. Joyce, and three anonymous reviewers for their comments that improved the manuscript. Funding was provided by the USGS Amphibian Research and Monitoring Initiative (ARMI) and the USGS Environments Program. This manuscript is ARMI contribution no. 698. Any use of trade, product, or firm names is for descriptive purposes only and does not imply endorsement by the U.S. Government.

References

- Arizona Department of Water Resources (ADWR) (2014) Climate of the San Rafael Basin. <http://www.azwater.gov/AzDWR/StatewidePlanning/WaterAtlas/SEArizona/Climate/SanRafael.htm>. Accessed 4 Aug 2017
- Arizona State Parks (n.d.) San Rafael State Natural Area: Ecological overview. <https://azstateparks.com/san-rafael/explore/science>. Accessed 4 Aug 2017
- Arst H (2003) Optical properties and remote sensing of multicomponental water bodies, Vol XII of marine science and coastal management. Springer Science Praxis, Ch 1
- Aspinall RJ, Marcus WA, Boardman JW (2002) Considerations in collecting, processing, and analysing high spatial resolution hyperspectral data for environmental investigations. *Journal of Geographical Systems* 4:15–29
- Bannari A, Pacheco A, Staenz K, McNairn H, Omari K (2006) Estimating and mapping crop residues cover on agricultural lands using hyperspectral and IKONOS data. *Remote Sensing of Environment* 104:447–459
- Boardman JW, Kruse FA, Green RO (1995) Mapping target signatures via partial unmixing of AVIRIS data, in: Green, RO (Ed), Summaries of the fifth annual JPL airborne earth science workshop. JPL Publication, Washington, pp 23–26, 95–1, Vol 1
- Campbell JB (1996) Introduction to remote sensing, 2nd edn. Taylor & Francis, London, p 622
- Chandler RB, Muths E, Sigafus BH, Schwalbe CR, Jarchow CJ, Hossack BR, Müller J (2015) Spatial occupancy models for predicting meta-population dynamics and viability following reintroduction. *Journal of Applied Ecology* 52:1325–1333
- Davies SJ, Clusella-Trullas S, Hui C, McGeoch MA (2013) Farm dams facilitate amphibian invasion: extra-limital range expansion of the painted reed frog in South Africa. *Austral Ecology* 38:851–863
- DeVries B, Huang C, Lang MW, Jones JW, Huang W, Creed IF, Carroll ML (2017) Automated quantification of surface water inundation in wetlands using optical satellite imagery. *Remote Sensing* 9(8). <https://doi.org/10.3390/rs9080807>
- Donchyts G, Baart F, Winsemius H, Gorelick N, Kwadijk J, Van De Giesen N (2016) Earth's surface water change over the past 30 years. *Nature Climate Change* 6(9):810–813
- Foody GM (2000) Estimation of sub-pixel land cover composition in the presence of untrained classes. *Computers and Geosciences* 26:469–478
- Frohn RC, D'Amico E, Lane C, Autrey B, Rhodus J, Liu H (2012) Multi-temporal sub-pixel Landsat ETM+ classification of isolated wetlands in Cuyahoga County, Ohio, USA. *Wetlands* 32:289–299
- Gallant A (2015) The challenges of remote monitoring of wetlands. *Remote Sensing* 7:10938–10950
- Gibbs JP (1993) Importance of small wetlands for the persistence of local populations of wetland-associated animals. *Wetlands* 13:25–31

- González-Bernal E, Greenlees M, Brown GP, Shine R (2012) Cane toads on cowpats: commercial livestock production facilitates toad invasion in tropical Australia. *PLoS One* 7:e49351
- Halabisky M, Moskal LM, Gillespie A, Hannam M (2016) Reconstructing semi-arid wetland surface water dynamics through spectral mixture analysis of a time series of Landsat satellite images (1984–2011). *Remote Sensing of Environment* 177:171–183
- Heinz DC, Chang CI (2001) Fully constrained least squares linear spectral mixture analysis method for material quantification in hyperspectral imagery. *IEEE Transactions on Geoscience and Remote Sensing* 39:529–545
- Hossack BR, Honeycutt RK, Sigafus BH, Muths E, Crawford CL, Jones TR, Sorensen JA, Rorabaugh JC, Chambert T (2017) Informing recovery in a human-transformed landscape: drought-mediated coexistence alters population trends of an imperiled salamander and invasive predators. *Biological Conservation* 209:377–394
- Hu YH, Lee HB, Scarpace FL (1999) Optimal linear spectral unmixing. *IEEE Transactions on Geoscience and Remote Sensing* 37:639–644
- Huang C, Peng Y, Lang M, Yeo I-Y, McCarty G (2014) Wetland inundation mapping and change monitoring using Landsat and airborne LiDAR data. *Remote Sensing of Environment* 141:231–242
- Ilori CO, Pahlevan N, Knudby A (2019) Analyzing performances of different atmospheric correction techniques for landsat 8: application for coastal remote sensing. *Remote Sensing* 11:469
- Jarchow CJ, Hossack BR, Sigafus BH, Schwalbe CR, Muths E (2016) Modeling habitat connectivity to inform reintroductions: a case study with the Chiricahua leopard frog. *Journal of Herpetology* 50: 63–69
- Jin H, Huang C, Lang MW, Yeo I-Y, Stehman SV (2017) Monitoring of wetland inundation dynamics in the Delmarva Peninsula using Landsat time-series imagery from 1985 to 2011. *Remote Sensing of Environment* 190:26–41
- Kalluri S, Gilruth P, Rogers D, Szczur M (2007) Surveillance of arthropod vector-borne infectious diseases using remote sensing techniques: a review. *PLoS Pathogens* 3:1361–1371
- Krausman PR, Rosenstock SS, Cain JW (2006) Developed waters for wildlife: science, perception, values, and controversy. *Wildlife Society Bulletin* 34:563–569
- Li L, Chen Y, Yu X, Liu R, Huang C (2015a) Sub-pixel flood inundation mapping from multispectral remotely sensed images based on discrete particle swarm optimization. *ISPRS Journal of Photogrammetry and Remote Sensing* 101:10–21
- Li L, Canters F, Solana C, Ma W, Chen L, Kervyn M (2015b) Discriminating lava flows of different age within Nyamuragira's volcanic field using spectral mixture analysis. *International Journal of Applied Earth Observation and Geoinformation* 40:1–10
- Lu D, Weng Q (2006) Use of impervious surface in urban land-use classification. *Remote Sensing of Environment* 102:146–160
- Mayes MT, Mustard JF, Melillo JM (2015) Forest cover change in Miombo woodlands: modeling land cover of African dry tropical forests with linear spectral mixture analysis. *Remote Sensing of Environment* 165:203–215
- McFeeters SK (1996) The use of the Normalized Difference Water Index (NDWI) in the delineation of open water features. *International Journal of Remote Sensing* 17:1425–1432
- Millennium Ecosystem Assessment (MEA) (2005) Ecosystems and human well-being: wetlands and water synthesis. Washington, DC, World Resources Institute
- Mitsch WJ, Gosselink JG (2007) Wetlands, 4th ed. Hoboken, New Jersey
- Moses WJ, Sterckx S, Montes MJ, De Keukelaere L, Knaeps E (2017) Atmospheric correction for inland waters. In: Bio-optical modeling and remote sensing of inland waters. Elsevier Inc., Amsterdam, pp 69–100
- Mundt JT, Streutker DR, Glenn NF (2007) Partial unmixing of hyperspectral imagery: theory and methods. *Proceedings of the American Society of Photogrammetry and Remote Sensing*, Tampa, Florida
- Nichol JE, Vohora V (2004) Noise over water surfaces in Landsat TM images. *International Journal of Remote Sensing* 25:2087–2093
- Nielsen AA (2001) Spectral mixture analysis: linear and semiparametric full and iterated partial unmixing in multi- and hyperspectral image data. *International Journal of Computer Vision* 42:17–37
- Papastergiadou ES, Retalis A, Apostolakis A, Georgiadis T (2007) Environmental monitoring of spatio-temporal changes using remote sensing and GIS in a Mediterranean wetland of northern Greece. *Water Resources Management* 22:579–594
- Pekel JF, Cottam A, Gorelick N, Belward AS (2016) High-resolution mapping of global surface water and its long-term changes. *Nature* 540:418–422
- Roshier DA, Rumbachs RM (2004) Broad-scale mapping of temporary wetlands in arid Australia. *Journal of Arid Environments* 56:249–263
- Rover J, Wylie BK, Ji L (2010) A self-trained classification technique for producing 30 m percent-water maps from Landsat data. *International Journal of Remote Sensing* 31:2197–2203
- Scheffer M, Zimmer K, Jeppesen E, Sondergaard M, Hanson M, Butler M, Declerck S, De Meester L (2006) Small habitat size and isolation can promote species richness: second-order effects on biodiversity in shallow lakes and ponds. *Oikos* 112:227–231
- Sun D, Liu N (2015) Coupling spectral unmixing and multiseasonal remote sensing for temperate dryland land-use/land-cover mapping in Minqin County, China. *International Journal of Remote Sensing* 36:3636–3658
- Tiner RW (1990) Use of high-altitude aerial photography for inventorying forested wetlands in the United States. *Forest Ecology and Management* 33/34:593–604
- Torbick N, Hession S, Hagen S, Wangwang N, Becker B, Qi J (2013) Mapping inland lake water quality across the lower peninsula of Michigan using Landsat TM imagery. *International Journal of Remote Sensing* 34(21):7607–7624
- U.S. Fish and Wildlife Service (USFWS) (2007) Chiricahua leopard frog (*Rana chiricahuensis*) final recovery plan. Albuquerque, New Mexico
- U.S. Geologic Survey (USGS) (2018) Product guide: Landsat 8 Surface Reflectance Code (LaSRC). Version 1.0, EROS data center. Available via <https://www.usgs.gov/media/files/landsat-8-surface-reflectance-code-lasrc-product-guide>. Accessed 12 May 2019
- Van Der Meer F (1999) Iterative spectral unmixing (ISU). *International Journal of Remote Sensing* 20:3431–3436
- Van Dyke E, Wasson K (2005) Historical ecology of a Central California estuary: 150 years of habitat change. *Estuaries* 28:173–189
- Wang D, Ma R, Xue K, Loiselle SA (2019) The assessment of Landsat-8 OLI atmospheric correction algorithms for inland waters. *Remote Sensing* 11:169
- Williams P, Whitfield M, Biggs J, Bray S, Fox G, Nicolet P, Sear D (2003) Comparative biodiversity of rivers, streams, ditches and ponds in an agricultural landscape in southern England. *Biological Conservation* 115:329–334